Zitierweise: *Angew. Chem. Int. Ed.* **2025**, e202503734
doi.org/10.1002/anie.202503734

Nanozymes

Transforming Chemiluminescence from Flash to Glow by Breaking the Catalytic Limitation with a Medium-Entropy Nanozyme

*Shuai Luo, Weiwei Chen, Yuru Wang, Wenrui Hu, Wencheng Xiao, Jie Wu, and Huangxian Ju**

Abstract: Intensive and persistent chemiluminescence (CL) emission is highly desired in biological imaging and is also a conundrum for most CL systems. Catalysts can efficiently improve the flash intensity but scarcely achieve persistent enhancement due to their catalytic limitation on CL reaction. Herein, a medium-entropy (ME) nanozyme with trinuclear configuration and a classical Prussian blue analogue (PBA) structure was designed to break the catalytic limitation. The ME PBA showed favorable enhancement on both flash and persistent CL emission of luminol-H_2O_2 system due to the recycling generation of catalytic center Co(II) through quick electron transfer among metal sites within framework, which provided a relatively stable CL emission enhanced by over two orders of magnitude in 1 h, achieving the transformation of CL from flash to glow. The CL enhancement and active valence cycle mechanism via intrareticular electron transfer were revealed by both experiments and density functional theory calculations. A facile CL imaging method was proposed to evaluate the bacterial motility, which demonstrated the application potential of the ME PBA. This work offers a new avenue to transform CL from flash to glow by breaking the catalytic limitation of nanozymes, which will conveniently expand their application in bioanalysis.

Introduction

Optical imaging as a powerful real-time monitoring tool has frequently appeared in biomedicine and bioassay, in which chemiluminescence (CL) imaging shows great practicality potential due to its high signal-to-background ratio[1] and simple operation. However, redox-based CL systems generally show ordinary performance in imaging due to the flash property or low luminous efficiency. Although some molecules such as *p*-bromophenol have been reported to assist horseradish peroxidase for prolonging the CL emission,[2] the fragility and high costs of natural enzyme hinder the further applications. Some strategies to slow the contact of CL reagents through in situ generation of H_2O_2 with local tandem catalysis[3] or restrain the diffusion of H_2O_2 with hydrogel[4] have also been reported. The former needs complex multiple-enzyme system, while the latter requires a H_2O_2 concentration of 0.1 M and high pH value, thus limiting their application in bioimaging. Another method to initiate the long-lasting CL of luminol is proposed by using hydroxyl radicals from H_2O_2 to produce π-conjugated carbon radicals at the π-network plane of graphene oxide.[5] Unfortunately, the CL emission can be endured only a few seconds, thus cannot meet the needs tracing biomolecules. Therefore, developing new strategies to achieve intensive and long-life CL emission has become an urgent project in bioimaging field.

The introduction of cascade resonance energy transfer (RET),[6] nanoconfinement,[7] or enzymatic reactions[8] is the common ways to enhance the CL emission. However, available RET system is limited, and the nanoconfinement of CL reagents in organic frameworks[7] is adverse to the persistence of CL emission. Some nanozymes including Cu^{2+}-modified nanoparticles,[8] mental oxides,[9] metal–organic frameworks,[10] and single-atom catalysts[11] exhibit CL enhancement activities and have been widely used to enhance the flash CL emission for sensitive detection of biomolecules, but they fail to prolong the CL emission for longtime tracing due to their self-limited behavior resulted from the adsorption of reaction products[12,13] or the consumption or conversion of the active sites.[13] The catalytic limitation of nanozymes often occurs in Fenton-like reactions,[14] in which Fe^{II} shows high activity to catalyze H_2O_2 with the generation of low-activity Fe^{III} that returns to Fe^{II} slowly, leading to decreasing catalytic efficiency. To ensure the durability of catalytic activity of nanozymes, the quick cycle of metal valence is critical. This has been achieved by nitrogen vacancies,[15] cocatalysts,[16] external light, or electricity.[17,18] However, these strategies cannot be used for long-life CL enhancement. Here, a medium-entropy (ME) trinuclear framework configuration was designed for achieving the quick cycle of metal valence by using Co(II) as the catalytic center and coexisting Ni(II) and Cu(II) to accelerate the cycle.

Medium entropy (ME) nanozymes are generally composed of various metal species, and their configurational

[*] S. Luo, Y. Wang, W. Hu, W. Xiao, J. Wu, Prof. H. Ju
State Key Laboratory of Analytical Chemistry for Life Science, School of Chemistry and Chemical Engineering, Nanjing University, Nanjing 210023, China
E-mail: hxju@nju.edu.cn
W. Chen
State Key Laboratory of Flexible Electronics, School of Chemistry and Life Sciences, Nanjing University of Posts and Telecommunications, Nanjing 210023, China

Additional supporting information can be found online in the Supporting Information section

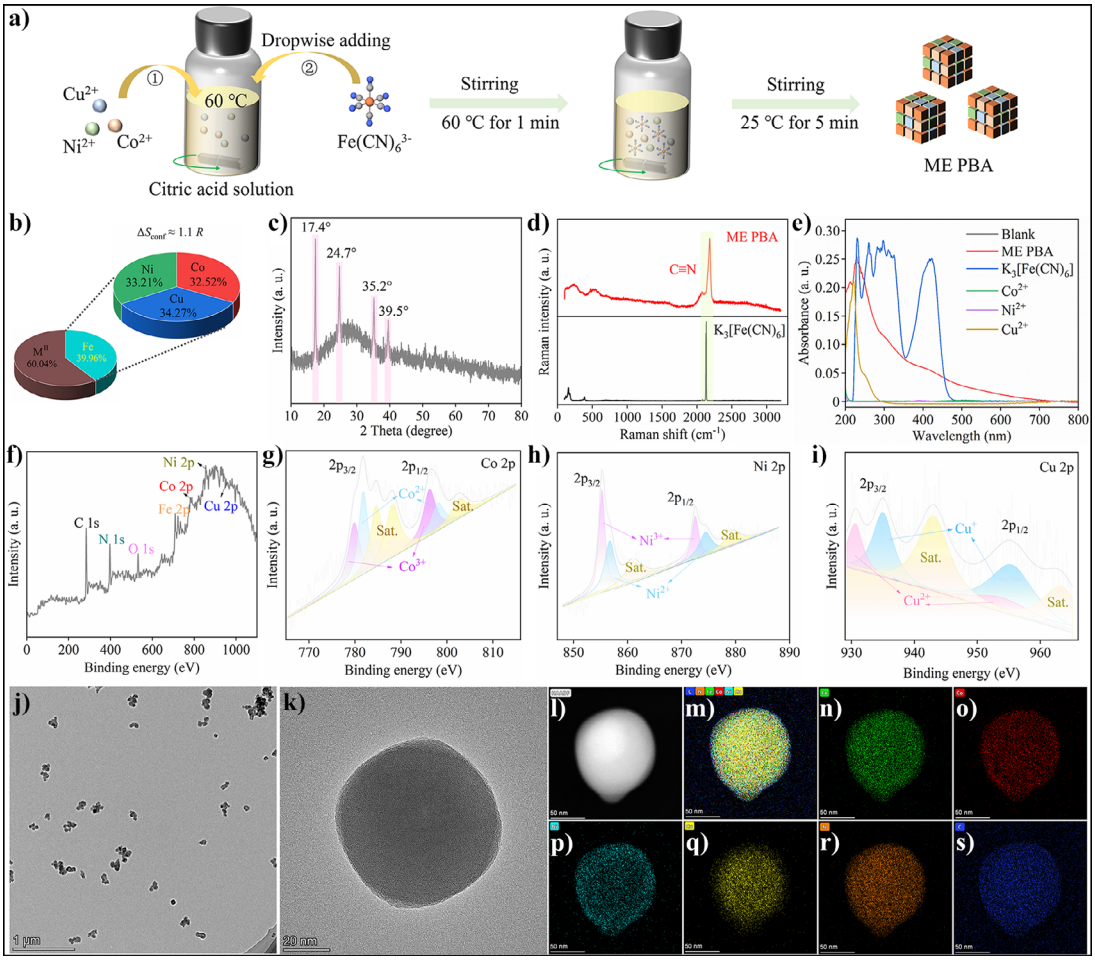

Figure 1. a) Scheme of preparation of ME PBA with a facile coprecipitation method. b) Atomic mole ratio of metal elements in ME PBA measured by ICP-OES. M^{II} means the introduced metal sources of Co, Ni, and Cu. c) XRD pattern of ME PBA. d) Raman spectra of ME PBA and $K_3[Fe(CN)_6]$. e) UV–vis spectra of ME PBA and original materials. f) Full scan, g) Co 2p, h) Ni 2p, and i) Cu 2p XPS spectra of ME PBA. j) and k) High-resolution TEM images of ME PBA. l) HADDF image of ME PBA. m)–s) EDS mapping of ME PBA m), and Fe n), Co o), Ni p), Cu q), N r), and C s) elements.

entropy is between 1.0 and 1.5 *R* (gas constant).[19] Their synthetic methods mainly derive from those for high-entropy alloys,[20] such as carbothermal shock synthesis,[21] laser scanning ablation,[22] and high-temperature oil bath.[23] These methods need harsh reaction processes or special apparatus. In view of the superiority of Prussian blue analogues (PBAs) constructed by the coordination between cyano groups and mental ions, such as easy preparation, abundant metal active centers, high porosity, massive defects, low toxicity, and favorable adjustability,[24,25] here a trinuclear framework was synthesized by introducing Co^{2+}, Ni^{2+}, and Cu^{2+} in PB structure (Figure 1a). The superiority of PBAs brought the enhanced catalytic activity[26] of the designed ME PBA. The intrareticular electron transfer (ET) among these metal ions, which can be achieved via exerting external light[27] or mechanical vitrification,[28] successfully broke the catalytic limitation to continuously generate reactive oxygen species (ROS) for persistently enhancing the emission of luminol by over two orders of magnitude. Moreover, the ME PBA achieved the transformation of intensive CL emission from flash to glow for 1 h due to the accelerated cycle of active valence. Using 4-mercaptophenyl-boronic acid linked ME PBA[29] to conjugate *Chromobacterium violaceum*[30] as a bacterial model, a facile CL imaging method was proposed for the evaluation of bacterial motility, related to the virulence and activity for invasion and proliferation,[31,32] demonstrating the favorable practicability of ME PBA.

Results and Discussion

Preparation and Characterizations of ME PBA

The catalytic limitation of nanozymes generally results in their limited durability, thus leads to a flash CL catalysis and severely obstructs the application of CL in biological imaging. To obtain intensive and long-life CL emission, a ME PBA was designed as nanozyme to break the catalytic limitation by using $K_3[Fe(CN)_6]$ to coprecipitate multiplex metal ions, such as Co^{2+}, Ni^{2+}, and Cu^{2+} (Figure 1a), because these metal ions are classical CL catalysts with respectable enhancement on flash emission[33] and also the potential metal nodes for the

construction of frameworks. This procedure formed a PBA framework structure through the coordination of cyano group with multiple metal ions, leading to the superior features of PBAs with an enhanced catalytic activity. The configuration entropy (ΔS_{conf}) of ME PBA, which is a critical factor to the definition for nanozymes of medium entropy,[19] was first calculated with following formula:[20]

$$\Delta S_{conf} = -R\sum_{i=1}^{n} x_i \ln x_i \quad (1)$$

where R and x_i represent gas constant and mole fraction of each component, respectively. According to the inductively coupled plasma-optical emission spectrometric (ICP-OES) analysis, the atomic mole ratios of Fe, Co, Ni, and Cu in ME PBA were about 2:1:1:1 (Figure 1b), which were identical to the results from energy dispersive spectrometric (EDS) mappings (Table S1), indicating that the introduced metal species occupied the same M^{II} sites in the framework. The configuration entropy was calculated to be 1.1 R, in the range of 1∼1.5 R for medium entropy.[19]

The structure of ME PBA was studied by X-ray diffraction (XRD) patterns, which showed four obvious peaks at 17.4°, 24.7°, 35.2°, and 39.5° (Figure 1c). These peaks could completely match with the characteristic XRD peaks of both binary FeCo, FeNi, and FeCu PBAs (Figure S1) and ternary FeCoNi, FeNiCu, and FeCoCu PBAs (Figure S2), illustrating a classical PBA structure. The slight difference among the peak positions of ternary PBAs was ascribed to the various metal species introduced in the framework (Figure S2). The special Raman peak of cyano group in the ME PBA could be observed at 2100∼2200 cm^{-1} (Figure 1d) and was slightly shifted in various PBAs due to the different coordinated M^{II} sites (Figure S3), revealing the presence of $M^{II}-NC-Fe^{III}$ structure. Moreover, the UV–vis spectra demonstrated that the original materials $[Fe(CN)_6]^{3-}$ and Cu^{2+} were successfully introduced into the structure of ME PBA (Figure 1e).

X-ray photoelectron spectroscopy (XPS) was carried out to reveal the element compositions and metal valences in ME PBA. The full scan spectrum of XPS revealed the presence of Fe, Co, Ni, Cu, C, and N elements in ME PBA (Figure 1f). The detailed XPS spectra of ME PBA indicated two valent forms of +2 and + 3 for Co and Ni elements (Figure 1g,h) and +1 and +2 for Cu element (Figure 1i). These variable valences of metal sites illustrated that the ET might occur in ME PBA framework, which is the potential evidence for clarifying the active valence cycle mechanism.

The high-resolution transmission electron microscopic (HRTEM) images of ME PBA exhibited a cube-like shape with a size of about ∼60 nm (Figure 1j,k). The shape was similar to those of FeCo, FeCu, FeCoCu, and FeNiCu PBAs (Figure S4), while FeNi and FeCoNi exhibited inferior shapes due to the effect metal sources. However, the HRTEM image did not show the lattice fringe (Figure 1j,k), which demonstrated the amorphous character of ME PBA due to the presence of multiple metal ions. The high-angle annular dark-field (HADDF) image and EDS mappings (Figures 1l–s and S5) showed the same elemental compositions as full scan spectrum of XPS, and all the elements distributed uniformly.

CL Properties and CL Imaging of ME PBA

For classical redox-based luminol-H_2O_2 CL system, free transition metal ions, particularly Co^{2+}, are frequently adopted as common catalysts to enhance the flash emission, and carbonate buffer solution (CBS) has been reported to efficiently boost the emission.[34] Thus, it is attractive to transform the feature of Co^{2+}-enhanced emission from flash to glow in CBS for CL imaging. As expected, the collected CL signal of ME PBA-luminol-H_2O_2 in CBS was much higher than those in other buffers and even strong alkalic solution (Figure 2a). Besides ME PBA, the flash CL emission catalyzed by free Co^{2+} ions and binary and ternary PBAs of Co element in CBS was also enhanced (Figure 2b). The CL enhancement was even greater than binary FeCu, FeNi, and ternary FeNiCu PBAs, demonstrating that Co site, not $[Fe(CN)_6]^{3-}$ in the framework, was indispensable for obviously enhancing the CL emission intensity. Moreover, both binary and ternary PBAs containing Co element showed much stronger CL emission than free Co^{2+}, illustrating that the coordination in PBA framework could effectively improve the catalytic activity. To exclude the effect of CL reagent depletion on flash CL emission, more luminol and H_2O_2 were added in the reaction solution, which did not recover the signal (Figure S6), further demonstrating the flash enhancement of Co-involved PBAs.

Different from the other PBAs, ME PBA exhibited a special CL kinetic curve (Figure 2c,d). Its flash CL signal appeared upon contacting luminol and H_2O_2 due to the rapid interaction of the surface Co sites with H_2O_2, and the intensity enhanced by 67.9 times (Figures 2c and S7), which was also higher than that of 50.9 times for free Co^{2+} catalysis (Figure 2b). The CL signal gradually increased for about 16 min and could maintain at the maximum emission till 60 min, indicating the remarkably improved durability. The glow CL emission boosted by ME PBA showed over 200-fold enhancement. The gradually increased CL intensity could be ascribed to the diffusion of H_2O_2 with a size of 3.886 Å × 4.281 Å × 2.860 Å (Figure S8) into the pore of framework with a size of about 5 Å × 5 Å[26] to react with internal Co sites for generating more ROS (Figure 2e), which then reacted with outside luminol molecules with a size larger than the pores (Figure S8). However, different from the mechanism reported previously,[4] the restrained H_2O_2 diffusion was not the main factor to prolong CL emission, which was demonstrated by the glow CL decrease of FeCo PBA with similar pores to ME PBA (Figure 2d).

To examine the effect of chemical component, $FeCoCu_2$ and $FeCoNi_2$ PBAs with the disorder degrees of Co similar to that in ME PBA were prepared. They failed to achieve satisfactory enhancement on glow CL (Figure S9), indicating that the presence of chemical effect to enhance glow CL. Meanwhile, the effect of entropy was examined using Fe(II)FeCoNiCu and MnFe(II)FeCoNiCu PBAs with higher entropies. They showed inferior enhancements on glow CL (Figure S10) to ME PBA, further demonstrating the superior configuration of ME PBA.

The CL imaging kinetic curve of ME PBA-luminol-H_2O_2 was similar to that obtained by flow injection, except

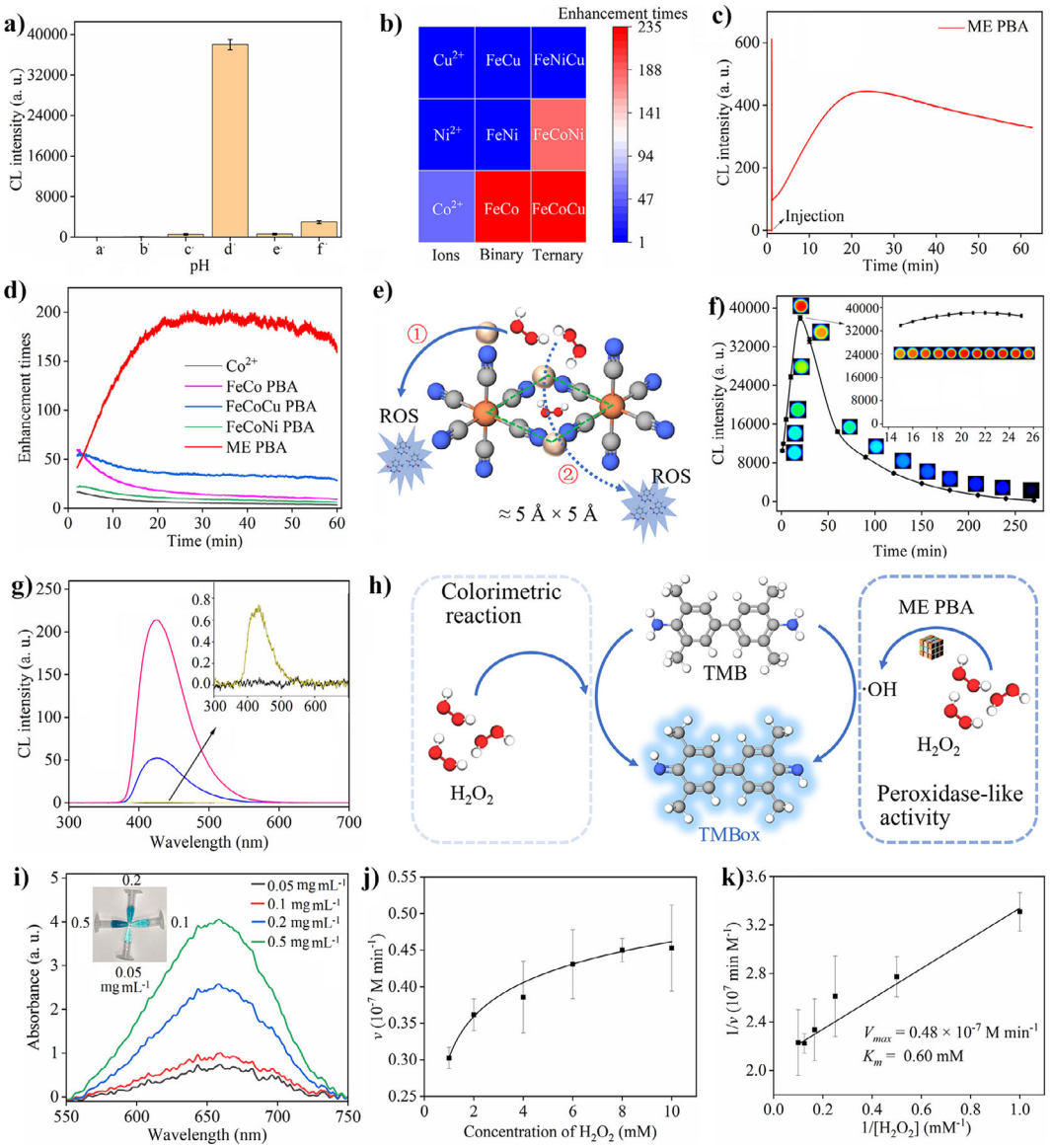

Figure 2. a) CL intensity of ME PBA-luminol-H_2O_2 in pH 7.4 PBS (a'), pH 9.0 PBS (b'), pH 9.0 Tris (c'), pH 9.0 CBS (d'), pH 10.0 NaOH (e'), and pH 11.0 NaOH (f'). $n = 3$. b) Enhancement times of flash CL signal with free metal ions and various PBAs. c) CL kinetic curve of ME PBA. d) Real-time enhancement times of CL signal by Co^{2+} and Co-involved PBAs. Note: the data in b), c), and d) were obtained by injection experiments. e) Schematic illustration of two reaction paths between H_2O_2 and ME PBA. f) CL imaging kinetic curve of ME PBA ($n = 3$). g) CL emission spectra of ME PBA-H_2O_2 (black), luminol-H_2O_2 (yellow), ME PBA (1.0 μg mL^{-1})-luminol-H_2O_2 (blue), and ME PBA (10 μg mL^{-1})-luminol-H_2O_2 (red). h) Schematic illustration of colorimetric reaction of TMB-H_2O_2-ME PBA. i) Absorption spectra of TMB-H_2O_2-ME PBA at 0.05, 0.1, 0.2 and 0.5 mg mL^{-1} ME PBA. j) Plot of reaction rate versus H_2O_2 concentration and k) double-reciprocal plot for measuring Michaelis constant of ME PBA with 10 mM TMB ($n = 3$).

the uncaptured primary flash peak (Figure 2f). ME PBA could persistently enhance the CL emission for at least 2 h, which could even be observed by naked eyes (Figure S11). After reaching the maximum emission, this system could remain at the maximum emission for more than ten minutes (inset in Figure 2f). Furthermore, the emission spectrum was the same as that of luminol with a peak at about 425 nm (Figure 2g), which did not occur in the absence of luminol, illustrating that the luminophore was luminol.

Enzyme-Like Activity of ME PBA

The peroxidase-like activity of transition metal PBAs has been described to decompose H_2O_2 with the generation of ROS (Figure S12).[35] Thus, TMB-H_2O_2 system was adopted to study the peroxidase-like activity of ME PBA (Figures 2h and S13). With the increasing ME PBA concentration, the absorbance of oxidized TMB (TMBox) increased (Figure 2i), which did not change in the absence of H_2O_2 (green line in Figure S13). From the reaction rates at different H_2O_2

concentrations, the Michaelis–Menten constant K_m could be obtained to be 0.60 mM by following equation:

$$1/v = K_m/v_{max}[H_2O_2] + 1/v_{max} \quad (2)$$

where v and v_{max} represent the initial and maximum reaction rate, respectively (Figure 2j,k). The v_{max} value was 0.48×10^{-7} M min^{-1}. Similarly, the K_m and v_{max} for FeCo, FeCoNi, and FeCoCu PBAs were 0.54, 0.62, and 0.44 mM and 4.8×10^{-8}, 6.2×10^{-8}, and 3.7×10^{-8} M min^{-1}, respectively (Figure S14). Moreover, ME PBA shows satisfactory stability upon the temperature change from 4 to 60 °C (Figure S15), providing a wide temperature range for enhancing the CL emission.

Mechanism of ME PBA for Enhancing and Prolonging CL Emission

The continuous production of ROS is a key factor to transform CL from flash to glow for prolonging the CL emission of luminol-H_2O_2 system. To uncover the mechanism, various scavengers, such as ascorbic acid, *p*-benzoquinone, and thiourea, were used to eliminate respectively total ROS, superoxide radical anion ($O_2^{\cdot-}$), and hydroxy radicals (·OH),[11,34] which can be generated by directly decomposing H_2O_2.[35] With the increasing scavenger concentration, the CL imaging signal attenuated (Figure 3a–c), indicating that both $O_2^{\cdot-}$ and ·OH played important roles in enhancing CL intensity. Moreover, the electron paramagnetic resonance (EPR) tests using DMPO as a trapping reagent successfully showed the signals of captured $O_2^{\cdot-}$ and ·OH radicals (Figure 3d), demonstrating the coexistence of $O_2^{\cdot-}$ and ·OH radicals in ME PBA-luminol-H_2O_2 system. As a member of ROS, singlet oxygen ($^1O_2$) has been reported to enhance the CL emission of luminol-based system.[36] Thus, tryptophan, a specific scavenger of $^1O_2$,[11] was added in ME PBA-luminol-H_2O_2 system, which resulted in the decrease of CL imaging signal (Figure S16), demonstrating that $^1O_2$ also existed in the CL reactions.

The constantly regenerated ROS for prolonging CL emission resulted from the persistent catalysis of ME PBA on decomposing H_2O_2 due to the active valence cycle of Co element between active Co^{2+} and inactive Co^{3+}.[37] Moreover, both FeCoNi and FeCoCu PBAs showed the enhancing and prolonging effects on CL emission compared with that in the absence of Ni or Cu element (Figures 2b,d), which could be ascribed to the valence cycles of Ni and Cu elements in the PBA framework. These cycles could be demonstrated by the presence of Ni^{3+} and Ni^{2+} in FeCoNi PBA (Figure S17) and Cu^{2+} and Cu^{+} in FeCoCu PBA (Figure S18), and the increase of Ni^{3+} and Cu^{2+} after ME PBA was treated with 0.2 M H_2O_2 for 1 h, which led to the increasing peak areas of Ni^{3+} and Cu^{2+} in the XPS spectra (Figure S19). Surprisingly, the treatment with 0.2 M H_2O_2 did not change the relative content of Co^{3+} and Co^{2+} in ME PBA, which showed a ratio of about 1:1 (Figure 3f), as that before the treatment (Figure 1g), indicating the presence of intrareticular ET among these metal ions for constantly decomposing H_2O_2. By contrary, the CL enhancement for all the combinations of free ions became weaker after flash emission, which did not show improved CL lifetime (Figure 3e), though the presence of Co^{2+} led to more than 10-times enhancement, illustrating the interactions among various free metal ions were negligible in their solutions.

To further probe the persistent CL emission mechanism, 0.2 M H_2O_2 was used to treat CoFe PBA for consuming the active Co sites in framework for 1 h. Different from ME PBA, which kept similar fractions of Co^{3+} and Co^{2+} (Figure 3f) and about 95% CL catalytic efficiency, the oxidized CoFe PBA showed increasing proportion of Co^{3+} species (Figure S20) and severely decreased performance at about 55% (Figure 3g). Meanwhile, the oxidation treatment did not affect the nonmetal element spectra of both ME PBA and CoFe PBA (Figures S19 and S21). These results demonstrated that the Ni and Cu atoms could quickly transfer electrons to surrounding oxidized Co atoms in the framework due to the high electric potential (1.8 V) of Co^{3+}/Co^{2+} pair,[38] which led to the regeneration of Co^{2+} species in the persistently catalytic process and thus broke the severe catalytic limitation commonly suffered in classical Fenton-like reaction.[14]

The ET process generally accompanies with the variation of charge. Density functional theory calculation was carried out to further uncover the mechanism of intrareticular ET. Bader charge analysis was carried out to inspect whether the charges of Co sites varied before (FeCo PBA) and after (ME PBA) the introduction of external metal species of Ni and Cu by using two constructed regular framework structures (Figure 3h,i). The calculated results showed all the Co sites in FeCo PBA with the same charges of 7.683 e. It illustrated that the intrareticular ET difficultly occurred among various Co sites in FeCo PBA. Even if the intrareticular ET occurred in the catalytic process to enhance the CL emission, the whole proportion of various valence state of Co did not change (one Co^{2+} to Co^{3+} must lead to another Co^{3+} to Co^{2+}). However, the random two Co sites in ME PBA were calculated as 7.685 e for Co-1 site and 7.687 e for Co-2 site. The results indicated that the introduction of Ni and Cu could increase the charges of Co sites in ME PBA, providing the evidence of ET from Ni and Cu to Co sites in the framework. Thus, the intrareticular ET among metal sites in ME PBA was verified to accelerate the active valence cycles and broke the catalytic limitation for transforming the CL from flash to glow.

As it was difficult to achieve the valence cycle of Co^{III}/Co^{II} pair with a high electric potential in Fenton-like reaction,[38] the decomposition of H_2O_2, catalyzed by Co^{2+} species in ME PBA, led to the primary flash CL signal (Figure 4a). The presence of Cu^{2+}/Cu^{+} with a relatively low electric potential (0.2 V) and a satisfactory Fenton-like reaction rate ($v = 4.6 \times 10^2$ M^{-1} s^{-1})[39] could enhance and prolong the CL emission through the persistent transfer electron from Cu^{+} species to inactive Co^{3+} to regenerate the active Co^{2+} in ME PBA framework. Meanwhile, Ni^{2+}, which was reported to easily lose electron to form Ni^{3+}, could also transfer electron to Co^{3+}[38] and Cu^{2+}[40] to regenerate active Fenton-like Co^{2+} and Cu^{+} species in ME PBA framework (Figure 4b). Thus, the active Co^{2+} could be

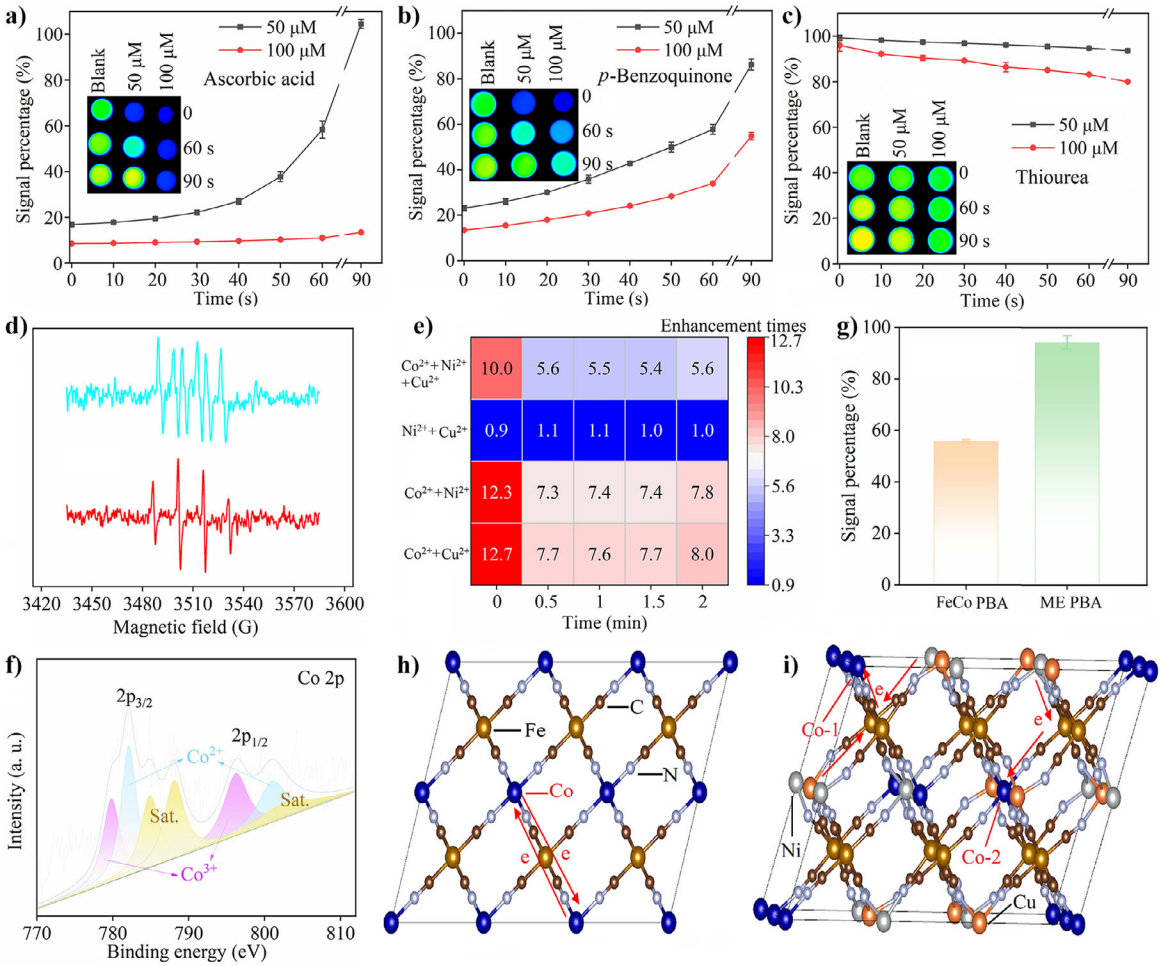

Figure 3. Quenching effects of a) ascorbic acid, b) *p*-benzoquinone, and c) thiourea on ME PBA-enhanced CL imaging signal ($n = 3$). d) EPR spectra of $O_2^{\cdot-}$ (cyan) and ·OH (red) in ME PBA-enhanced CL system. e) CL enhancement times at different time points by the combinations of $Co^{2+} + Cu^{2+}$, $Co^{2+} + Ni^{2+}$, $Ni^{2+} + Cu^{2+}$, and $Co^{2+} + Ni^{2+} + Cu^{2+}$. f) XPS spectrum of Co 2p of ME PBA after treated with 0.2 M H_2O_2. g) Signal change of FeCo PBA and ME PBA after treated with H_2O_2 ($n = 3$). Crystal structures of h) FeCo PBA and i) ME PBA for Bader charge calculations to uncover the ET among metal sites through cyano bridge. The red arrows represent the potential paths of ET.

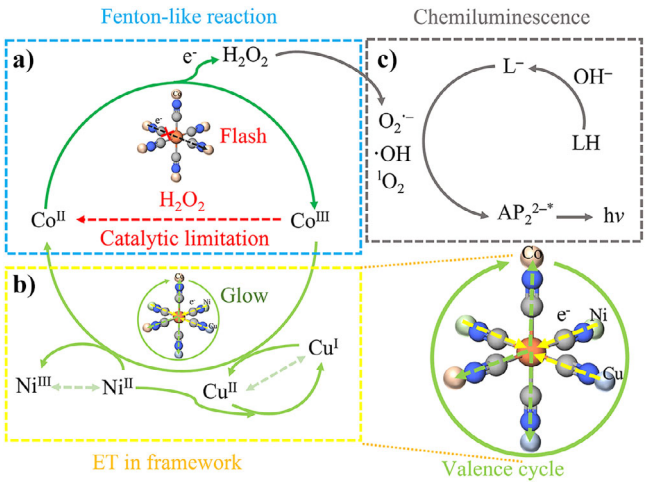

Figure 4. a) Schematic illustration of Fenton-like reaction process of Co species. b) The regeneration of active valence of Co through ET in framework of ME PBA. c) Schematic process of ME PBA-participated CL reaction.

constantly regenerated to persistently enhance CL emission (Figure 4c).

CL Imaging Application in Evaluating Bacterial Motility

To verify the application potential of ME PBA-luminol-H_2O_2 system with intensive and long-life CL emission in CL imaging analysis, it was used to dynamically evaluate the motility of bacteria, which is a key virulence factor for invasion and proliferation, and is conventionally evaluated by constructing genetic engineering to express fluorescent proteins in bacteria.[41] Using *C. violaceumon*, whose metabolite violacein possesses potential antitumor and antiviral properties, as a target, a CL imaging method was proposed (Figure 5a). Both ME PBA and CL reagents, such as luminol and H_2O_2, did not obviously influence the growth activity of *C. violaceumon* (Figure S22), showing acceptable biotoxicity. After 4-mercaptophenylboronic acid was linked to ME PBA by continuously stirring to covalently bind the cell wall of bacteria (Figure S23),[29] the conjugate showed the CL

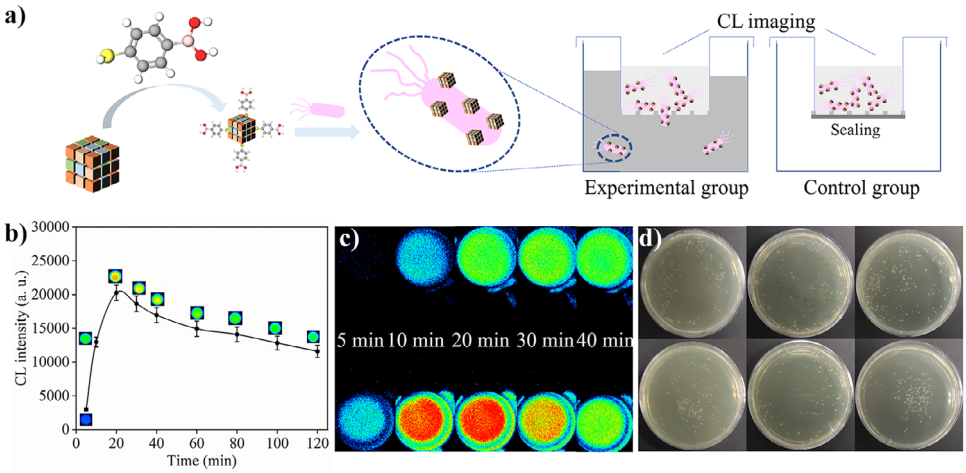

Figure 5. a) Schematic illustration of CL imaging for dynamic evaluation of bacterial motility. b) CL imaging kinetic curve of ME PBA after linking with 4-mercaptophenylboronic acid ($n = 3$). c) CL images of control (upper) and experimental (below) groups at different collection times. d) Photos for plate counting of bacterial colonies before (upper) and after (below) motility evaluation for 40 min.

imaging property similar to ME PBA (Figures 5b and S24). Thus, this proposed method was feasible for bacterial motility evaluation. The bacterial motility detected with CL imaging showed negligible influence of glucose concentration on the nutritional tendency feature of bacteria (Figure S25), ensuring its accuracy.

The accuracy was demonstrated with a control group and plate counting of bacterial colonies. The same signal of experimental group as that of control group with 50% of the ME PBA-bacteria conjugate was observed at 40 min (Figure 5c), indicating the migration of *C. violaceumon* with the corresponding percentage to the well of 24-well cell culture plate, which was close to the average percentage of 49.8% obtained from plate counting method with an RSD of 3.5% (Figure 5d). During 40-min monitoring, the motility of *C. violaceumon* was about 4.5×10^3 cfu min^{-1}. Its limit of detectable motility was calculated to be 2.4×10^3 cfu min^{-1}. The general applicability of the constructed method was verified using *Escherichia coli* BL21(DE3) and K12 strains. The motility of *E. coli* BL21(DE3) strain was tested as 6.5×10^3 cfu min^{-1} (Figure S26), while the motility of *E. coli* K12 strain was 5.7×10^3 cfu min^{-1} (Figure S27). Compared with traditional genetic engineering method, the CL imaging method constructed for evaluating bacterial motility exhibited the merits of convenience, simplicity and low time consumption. Therefore, the ME PBA possessed favorable application potential in CL bioassay.

Conclusions

In conclusion, a strategy for prolonging the intensive CL emission of luminol-H_2O_2 system was designed by breaking the catalytic limitation of nanozyme, which was achieved by constructing a nanozyme of ME PBA with a trinuclear configuration of Co, Ni, and Cu in Prussian blue framework. ME PBA with improved catalytic activity strongly enhanced both the flash and persistent CL emission due to the coordination of cyano groups with multiple metal ions, which quickly regenerated active Co^{2+} species through intrareticular ET from Ni^{2+} and Cu^{+} to Co^{3+} for accelerating the valence cycle of Co^{III}/Co^{II} pair, and thus constantly decomposed H_2O_2 to generate ROS. Benefiting from the favorable capability of ME PBA in CL imaging, a facile CL imaging method was proposed to evaluate the bacterial motility. The method exhibited favorable convenience, simplicity, and short-time consumption. This proof-of-principle work opens an avenue to break the catalytic limitation of nanozymes for persistent catalysis and transform enhanced CL from flash to glow for meeting the needs in bioimaging and bioanalysis.

Supporting Information

Experimental methods and computational details have been supplied in Supporting Information. The authors have cited additional references within the Supporting Information.[42–49]

Acknowledgements

This work was financially supported by the National Natural Science Foundation of China (21827812, 21890741).

Conflict of Interests

The authors declare no conflict of interest.

Data Availability Statement

The data that support the findings of this study are available from the corresponding author upon reasonable request.

Keywords: Catalytic limitation • Chemiluminescence • Chemiluminescence imaging • Medium-entropy nanozyme • Persistent emission • Valence

[1] J. Zhang, C. Wickizer, W. H. Ding, R. Van, L. Y. Yang, B. Y. Zhu, J. Yang, Y. L. Wang, Y. L. Wang, Y. L. Xu, C. Zhang, S. Q. Shen, C. N. Wang, Y. H. Shao, C. Z. Ran, *Proc. Natl. Acad. Sci. USA* **2023**, *120*, e2310131120.
[2] J. Li, X. Zhao, L.-J. Chen, H.-L. Qian, W.-L. Wang, C. Yang, X.-P. Yan, *Anal. Chem.* **2019**. *91*, 13191–13197.
[3] P. Y. Dang, X. Liu, H. X. Ju, J. Wu, *Anal. Chem.* **2020**, *92*, 5517–5523.
[4] Y. Liu, W. Shen, Q. Li, J. Shu, L. Gao, M. Ma, W. Wang, H. Cui, *Nat. Commun.* **2017**, *8*, 1003.
[5] L. Yang, R. L. Zhang, B. H. Liu, J. P. Wang, S. H. Wang, M. Y. Han, Z. P. Zhang, *Angew. Chem. Int. Ed.* **2014**, *53*, 10109–10113.
[6] Q. Song, X. N. Yan, H. Cui, M. M. Ma, *ACS Nano* **2020**, *14*, 3696–3702.
[7] A. Lyu, Y. S. Wang, H. Cui, *Anal. Chem.* **2023**, *95*, 7914–7923.
[8] S. Wang, R. Cazelles, W. C. Liao, M. Vázquez-González, A. Zoabi, R. Abu-Reziq, I. Willner, *Nano Lett.* **2017**, *17*, 2043–2048.
[9] Q. Y. Li, M. X. Sun, Y. Y. Su, K. X. Zhang, Y. Lv, *Sens. Actuator B-Chem.* **2021**, *339*, 129876.
[10] Y. Wu, Y. L. Qin, M. Muppidathi, R. Carmieli, M. Fadeev, W. Lei, M. Z. Xia, I. Willner, *Adv. Funct. Mater.* **2024**, *34*, 2306929.
[11] S. Luo, J. Q. Gao, J. X. Xian, H. Ouyang, L. Wang, Z. F. Fu, *Anal. Chem.* **2022**, *94*, 13533–13539.
[12] W. J. Luo, C. F. Zhu, S. Su, D. Li, Y. He, Q. Huang, C. H. Fan, *ACS Nano* **2010**, *4*, 7451–7458.
[13] M. Zandieh, J. W. Liu, *ACS Nano* **2021**, *15*, 15645–15655.
[14] Z. J. Wang, Y. Du, P. Zhou, Z. K. Xiong, C. S. He, Y. Liu, H. Zhang, G. Yao, B. Lai, *Chem. Eng. J.* **2023**, *454*, 140096.
[15] L. N. Su, P. F. Wang, X. L. Ma, J. H. Wang, S. H. Zhan, *Angew. Chem. Int. Ed.* **2021**, *60*, 21261–21266.
[16] M. Y. Xing, W. J. Xu, C. C. Dong, Y. C. Bai, J. B. Zeng, Y. Zhou, J. L. Zhang, Y. D. Yin, *Chem* **2018**, *4*, 1359–1372.
[17] X. X. Qiao, X. J. Liu, W. Y. Zhang, Y. L. Cai, Z. Zhong, Y. F. Li, J. Lu, *Sep. Purif. Technol.* **2021**, *279*, 119760.
[18] C. Wang, W. F. Zhang, J. W. Wang, P. Xia, X. G. Duan, Q. He, I. Sirés, Z. H. Ye, *Appl. Catal., B* **2024**, *342*, 123457.
[19] G. H. Han, M. G. Li, H. Liu, W. Y. Zhang, L. He, F. Y. Tian, Y. Q. Liu, Y. S. Yu, W. W. Yang, S. J. Guo, *Adv. Mater.* **2022**, *34*, 2202943.
[20] E. P. George, D. Raabe, R. O. Ritchie, *Nat. Rev. Mater.* **2019**, *4*, 515–534.
[21] Y. G. Yao, Z. N. Huang, P. F. Xie, S. D. Lacey, R. J. Jacob, H. Xie, F. J. Chen, A. Nie, T. C. Pu, M. Rehwoldt, D. W. Yu, M. R. Zachariah, C. Wang, R. Shahbazian-Yassar, J. Li, L. B. Hu, *Science* **2018**, *359*, 1489–1494.
[22] B. Wang, C. Wang, X. W. Yu, Y. Cao, L. F. Gao, C. P. Wu, Y. F. Yao, Z. Q. Lin, Z. G. Zou, *Nat. synth.* **2022**, *1*, 138–146.
[23] C. H. Zhan, Y. Xu, L. Z. Bu, H. Z. Zhu, Y. G. Feng, T. Yang, Y. Zhang, Z. Q. Yang, B. L. Huang, Q. Shao, X. Q. Huang, *Nat. Commun.* **2021**, *12*, 6261.
[24] S. Luo, J. Q. Gao, H. W. Yuan, J. Yang, Y. H. Fan, L. Wang, H. Ouyang, Z. F. Fu, *Anal. Chem.* **2023**, *95*, 9366–9372.
[25] M. Vázquez-González, R. M. Torrente-Rodríguez, A. Kozell, W.-C. Liao, A. Cecconello, S. Campuzano, J. M. Pingarrón, I. Willner, *Nano Lett.* **2017**, *17*, 4958–4963.
[26] X. Y. Meng, J. Y. Yang, C. C. Zhang, Y. F. Fu, K. Li, M. H. Sun, X. G. Wang, C. Z. Dong, B. C. Ma, Y. Ding, *ACS Catal.* **2022**, *12*, 89–100.
[27] M. Cammarata, S. Zerdane, L. Balducci, G. Azzolina, S. Mazerat, C. Exertier, M. Trabuco, M. Levantino, R. Alonso-Mori, J. M. Glownia, S. Song, L. Catala, T. Mallah, S. F. Matar, E. Collet, *Nat. Chem.* **2021**, *13*, 10–14.
[28] S. Kosasang, N. Ma, S. Impeng, S. Bureekaew, Y. Namiki, M. Tsujimoto, T. Saothayanun, H. Yamada, S. Horike, *J. Am. Chem. Soc.* **2024**, *146*, 17793–17800.
[29] H. Y. Wang, Y. F. Zhou, X. X. Jiang, B. Sun, Y. Zhu, H. Wang, Y. Y. Su, Y. He, *Angew. Chem. Int. Ed.* **2015**, *54*, 5132–5136.
[30] M. Venkatramanan, E. Nalini, *Front. Microbiol.* **2024**, *15*, 1303595.
[31] C. Josenhans, S. Suerbaum, *Int. J. Med. Microbiol.* **2002**, *291*, 605–614.
[32] K. Abe, N. Koizumi, S. Nakamura, *Nat. Commun.* **2023**, *14*, 7703.
[33] S. Luo, J. Q. Gao, Y. Chen, H. Ouyang, L. Wang, Z. F. Fu, *Talanta* **2022**, *250*, 123732.
[34] T. H. Zheng, W. Nie, L. Yu, J. N. Shu, Y. H. Li, C. L. Tian, W. Wang, H. Cui, *Proc. Natl. Acad. Sci. USA* **2022**, *119*, e2207693119.
[35] L. Tian, Z.-J. Tang, L.-Y. Hao, T. Dai, J.-P. Zou, Z.-Q. Liu, *Angew. Chem. Int. Ed.* **2024**, *63*, e202401434.
[36] L. Li, X. Zhang, Y. Ren, Q. Yuan, Y. Wang, B. Bao, M. Li, Y. Tang, *J. Am. Chem. Soc.* **2024**, *146*, 5927–5939.
[37] T. G. Burdo, W. R. Seitz, *Anal. Chem.* **1975**, *47*, 1639–1643.
[38] P. C. Cai, J. Zhao, X. H. Zhang, T. Y. Zhang, G. M. Yin, S. Chen, C. L. Dong, Y. C. Huang, Y. Y. Sun, D. J. Yang, B. S. Xing, *Appl. Catal., B* **2022**, *306*, 121091.
[39] Z. Q. Zhu, L. Wang, W. Zhang, C. Hou, C. Y. Wang, J. C. Zhao, *Chem. Eng. J.* **2024**, *481*, 148313.
[40] H. Wang, M. M. Jing, Y. Wu, W. L. Chen, Y. Ran, *J. Hazard. Mater.* **2018**, *353*, 53–61.
[41] J. Xu, N. Koizumi, S. Nakamura, *Front. Microbiol.* **2020**, *11*, 1886.
[42] X. X. Mao, F. N. He, D. H. Qiu, S. J. Wei, R. G. Luo, Y. Chen, X. B. Zhang, J. P. Lei, D. Monchaud, J. L. Mergny, H. X. Ju, J. Zhou, *Anal. Chem.* **2022**, *94*, 7295–7302.
[43] J. X. Xian, S. Luo, J. X. Xue, L. X. Zhang, Z. F. Fu, H. Ouyang, *Anal. Chem.* **2022**, *94*, 11449–11456.
[44] G. Kresse, J. Furthmüller, *Comput. Mater. Sci.* **1996**, *6*, 15–50.
[45] G. Kresse, J. Furthmüller, *Phys. Rev. B* **1996**, *54*, 11169–11186.
[46] J. P. Perdew, K. Burke, M. Ernzerhof, *Phys. Rev. Lett.* **1996**, *77*, 3865–3868.
[47] G. Kresse, D. Joubert, *Phys. Rev. B* **1999**, *59*, 1758–1775.
[48] P. E. Blöchl, *Phys. Rev. B* **1994**, *50*, 17953–17979.
[49] S. Grimme, J. Antony, S. Ehrlich, H. Krieg, *J. Chem. Phys.* **2010**, *132*, 154104.

Manuscript received: February 14, 2025
Revised manuscript received: May 19, 2025
Accepted manuscript online: July 28, 2025
Version of record online: ■■, ■■